Supplemental Material

Switching on Superferromagnetism

A. Arora[1,*], L. C. Phillips[2,*], P. Nukala[3], M. Ben Hassine[3], A.A. Ünal[1], B. Dkhil[3], Ll. Balcells[4], O. Iglesias[5] A. Barthélémy[2], F. Kronast[1], M. Bibes[2], and S. Valencia[1,†]

[1]Helmholtz-Zentrum Berlin fur Materialien und Energie, Albert-Einstein-Str. 15, D-12489 Berlin, Germany

[2]Unite Mixte de Physique, CNRS, Thales, Univ. Paris-Sud, Universite Paris-Saclay, 91767 Palaiseau, France

[3]Laboratoire SPMS, UMR 8580, Ecole Centrale Paris-CNRS, Grande voie des vignes, Châtenay-Malabry 92290, France

[4]Institut de Ciència de Materials de Barcelona (ICMAB-CSIC), Campus de la U.A.B. 08193 Belltaterra, Spain

[5]Department of Condensed Matter Physics and Institute of Nanoscience and Nanotechnology (IN[2]UB), University of Barcelona, Av. Diagonal 647, 08028 Barcelona, Spain

[*]These authors contributed equally to this work.

[†] Corresponding author: sergio.valencia@helmholtz-berlin.de

1.-Azimuthal dependence of the XMCD: Magnetic orientation of Fe domains on BTO

Within the tetragonal phase of BTO FE a_1 and a_2 domains introduce 1.1% uniaxial lattice strain along $[010]_{pc}$ and $[100]_{pc}$ with respect to strain-free *c* FE domains. This strain is expected to be partially or totally transferred to the Fe film deposited on top leading to changes on the magnetoelastic anisotropy. If the magnetoelastic anisotropy dominates over other sources of anisotropy, the local magnetic easy axis, and so the magnetization direction[1, 2], are expected to lay either along $[010]_{pc}$ or $[100]_{pc}$.

Within this work we use X-ray magnetic circular dichroism (XMCD) as magnetic contrast mechanism so to “visualize” and characterize magnetic domains on Fe, i.e. their shape, orientation and evolution as the voltage applied across the FE BTO substrate is changed. XMCD is proportional to the projection of the magnetization ($\vec{M}$) along the beam propagation direction ($\vec{k}$), i.e.

$$XMCD \propto \vec{k} \cdot \vec{M} = |\vec{k}| \cdot |\vec{M}| \cdot \cos\left(\widehat{\vec{k} \cdot \vec{M}}\right).$$

The strength of the XMCD for a given magnetic domain does not depend only on an intrinsic property such as $|\vec{M}|$ but also on the experimental geometry as $\widehat{\vec{k} \cdot \vec{M}}$ which can be changed by an azimuthal rotation of the sample. Within this context an XMCD = 0 is ambiguous as it could arise from i) $|\vec{M}|$ = 0 or ii) $\cos\left(\widehat{\vec{k} \cdot \vec{M}}\right)$ i.e. $\vec{M} \perp \vec{k}$. Figure 3 of the main text shows different regions on the XMCD image having XMCD = 0 (white color). To disentangle their origin we have obtained XMCD images at two different azimuth angles, i.e. ⍰ = 0° ($\vec{k}$ ∥ $[100]_{pc}$) and ⍰ = 90° ($\vec{k}$ ∥ $[010]_{pc}$), see Figure S1

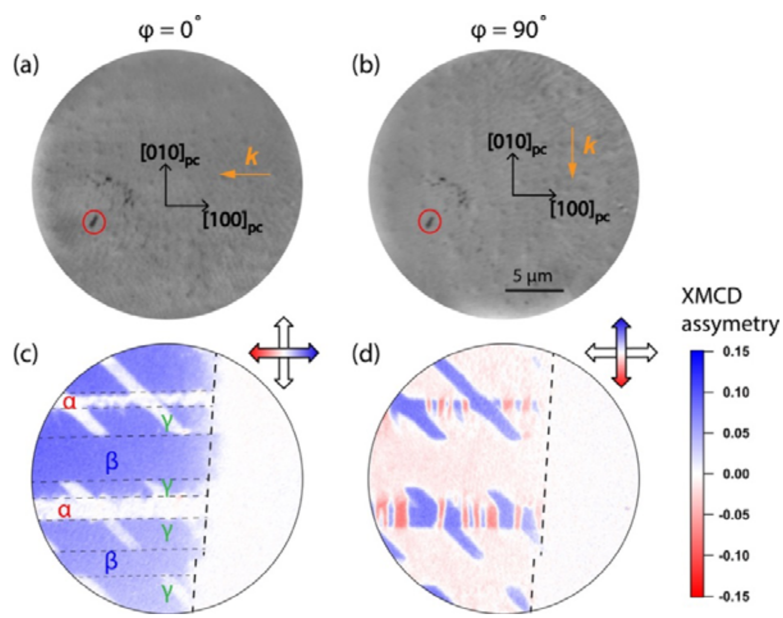

Figure S1 XAS (a-b) and corresponding XMCD-PEEM images (c-d) obtained at the Fe L_3-edge (707.8 eV) at T=320 K, V=170V and at different azimuthal angles (⍰), as indicated. Images have been rotated so to facilitate comparison. Red circle in panels (a-b) highlights the same deffect. Orange arrows in panels (a) and (b) indicate the direction of propagation of the radiation, parallel to $[100]_{pc}$ for ⍰=0° and parallel to $[010]_{pc}$ for ⍰=90°, respectively . Dashed line in panels (c-d) indicates the onset of long-range FM ordering along the wedge. Red-white-blue crosses on right side of images (c) and (d) indicate the expected XMCD contrast depending on the direction of the magnetization vector.

The sample region at the right hand side of the black dashed line along $[010]_{pc}$ (t_{Fe} < 1.3 nm, see Figure 1) depicted in panels c-d shows no XMCD contrast independent of φ highlighting the absence of long-range ferromagnetic order ($|\vec{M}|$ = 0) within this region. On the contrary the XMCD strongly depends on φ for t_{Fe} > 1.3 nm (left hand side of black dashed line);

- Magnetic domain regions labelled α for = 0° shows no XMCD. An azimuthal rotation of 90° shows a clear XMCD magnetic contrast for these very same regions. Indeed the XMCD for = 90° highlights that α domains are composed of smaller magnetic domains with the direction of their magnetization oriented alternatively along $[010]_{pc}$ and $[0\bar{1}0]_{pc}$.

- Magnetic domain regions labelled β for = 0° shows homogeneous blue-coloured XMCD which almost vanishes for = 90°. Hence the magnetization direction of β domains is oriented along $[100]_{pc}$. The faint red contrast still present at = 90° indicates that the azimuthal rotation angle is not exactly 90° as intended but close to it

- Magnetic domain regions labelled γ for = 0° shows blue/white-coloured XMCD. Blue (white) coloured XMCD region behaves as β (α) domains when changing the azimuth angle of the sample highlight the orientation of their magnetization along $[100]_{pc}$ ($[010]_{pc}$).

An intermediate azimuth angle of 45° where $\vec{k} \parallel [110]_{pc}$ warrants a non-zero (and equal in amplitude) projection of the magnetization along the beam propagation direction for both, magnetic domains with magnetization direction parallel to $[100]_{pc}$ and $[010]_{pc}$, see Figure S2.

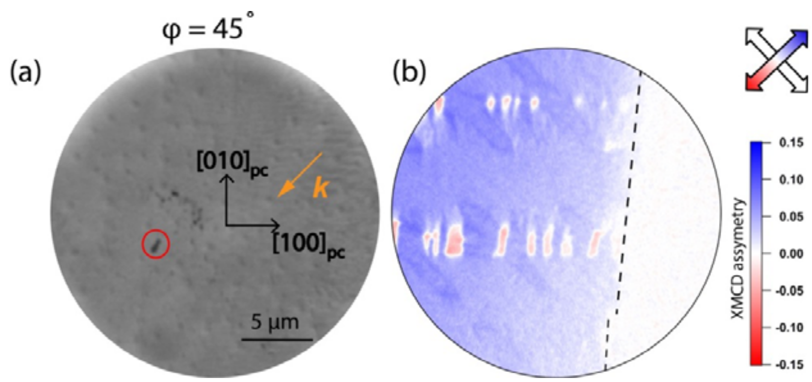

Figure S2 XAS (a) and corresponding XMCD-PEEM image (b) obtained at the Fe L_3-edge (707.8 eV) at T=320 K, V=170V at an azimuthal angles = 45°. Red circle in panels a highlghts the same deffect as in panels (a) and (b) of Figure S1. Orange arrow in panel a indicate the direction of propagation of the radiation, parallel to $[110]_{pc}$. Black dot line in panel d indicates the onset of long-range FM ordering along the wedge. Red-white-blue crosses on right side of images (b) indicates the expected XMCD contrast depending on the direction of the magnetization vector.

2.- Effective magnetostriction and correlation between XMCD and FE BTO domains for the virgin state

In magnetoelastic systems for which the magnetoelastic anisotropy dominates over other anisotropies the sign of the magnetostriction constant (λ) allows to predict whether the spontaneous magnetization of Fe orients along or orthogonal to the applied strain[2]. Vice versa, the observation of a rotation of the magnetization orientation under a known strain allows to determine the sign of λ. While the magnetostriction constant is considered to be positive for epitaxial Fe films it is assumed to be negative for polycrystalline samples[3, 4]. For the latter however, several factors such as the texture and/or intergranular interactions might lead to a change of sign for λ (Ref. 5). Here we consider that the Fe layer, although partially oxidized at its interface with $BaTiO_3$ behaves as a single layer with an effective magnetostriction constant λ which sign is empirically determined as described in the following.

XMCD images for decreasing voltages from +170 V to -170 V have been obtained at an azimuth angle ?=45° allowing magnetic sensitivity to α, β, and γ FM domains. While at ±170 V a pure FE c-domain state for BTO is expected, the coexistence of a_1 and *c* FE domains at voltages close to zero is anticipated[1, 2, 6]. Figure 4 (within the main text) shows XMCD images obtained at +170 V (a), 0 V (b) and -170 V (c), respectively. We observe that FM α domains nucleate and grow when decreasing V from + 170 V to 0 V and decrease and disappear when approaching –170 V. This behaviour is alike to that expected for FE a_1 domains which disappear (appear) at high (low) values of $|V|$ at expenses of *c* FE domains. Hence we conclude that the FE domains underlying these α regions are a_1.

The magnetization direction within this α regions coincides with the direction of the elongated *a* axis of the underlying a_1 FE domains (see section 1 of S.I.) as the latter is orthogonal to the $[100]_{pc}$ FE domain walls. As the magnetization of this new α regions is parallel to the direction of local uniaxial tensile strain (see also section 3 of S.I.) we can conclude that the magnetostriction constant has a positive sign.

3.- Differential strain analysis

The empirical knowledge of the sign of the magnetostriction and the voltage dependent FM domain imaging allows, to some extent, to reconstruct the local FE domain history of BTO. We assume that the Fe behaves as a single layer with positive magnetostriction constant, and that the magnetic orientation is not significantly affected by reconstruction processes (creep, surface morphology changes) on the time scale of our experiment. Then the voltage-induced local elastic modulation of magnetic domain patterns can be explained by the difference between the two in-plane normal strain components for the FM film, i.e. $\bar{\varepsilon}^{FM} = {\varepsilon^{FM}}_{[010]_{pc}} - {\varepsilon^{FM}}_{[100]_{pc}}$ and its effect on the magnetic anisotropy[2]. In the present case, with Fe having a positive sign for the magnetostriction, $\bar{\varepsilon}^{FM}$ determines the orientation of the magnetic easy axis so that $\bar{\varepsilon}^{FM} > 0$ and $\bar{\varepsilon}^{FM} < 0$ lead to magnetic easy axis oriented along $[010]_{pc}$ and $[100]_{pc}$, respectively.

The magnetic domain pattern imprinted on Fe does not only depend on the (differential) strain of the underlying FE domains ($\bar{\varepsilon}^{BTO} = 0, +1.1, -1.1\%$ for *c,* a_1, and a_2 FE domains, respectively) at a given V but also on the strain history[1, 2, 7, 8] i.e. $\bar{\varepsilon}^{FM} = \bar{\varepsilon}^{FM}_{growth} + \Delta\bar{\varepsilon}^{FM}$, with $\bar{\varepsilon}^{FM}_{growth}$ the differential strain induced on Fe at growth time and $\Delta\bar{\varepsilon}^{FM} \propto \quad (\bar{\varepsilon}^{BTO} - \bar{\varepsilon}^{BTO}_{growth})$.

Strain transfer from the ferroelectric substrate to the FM thin film can originate during i) film [1, 7-9], ii) temperature variation leading to FE phase transitions[8, 10] and, iii) application of voltage inducing FE domains switching[1]. For cases ii) and iii) there is a full transfer of strain from the FE substrate to the FM film[8]. On the contrary, the strain transfer at growth time has been reported to be small[1, 7, 8], i.e. $\bar{\varepsilon}^{FM}_{growth} \; = \delta \;\; \bar{\varepsilon}^{BTO}_{growth}$ with $0 < \delta < 0.1$. In the following we introduce following notation so to identify FE BTO domains after growth time (c^{gr}, a_1^{gr}, a_2^{gr}), after thermal cycling (c^{T}, a_1^{T}, a_2^{T}) and after voltage application (c^{V}, a_1^{V}, a_2^{V}).

It has been shown that at RT the combination of these three mechanisms can lead, for FM thin films deposited on top of BTO, to magnetic domain patterns where one or two of α, β and γ FM domain types coexist[1, 2, 7, 8]. To this respect the fact that we observe coexistence of all 3 magnetic configurations might seem surprising. However, its simultaneous presence as well as their evolution with the application of voltage can be explained by identifying the FE domain states for BTO before (at growth time) and after the thermal cycle.

Figure 1(f) (within main text) shows no imprint of underlying FE domains on the magnetic domain pattern of Fe after growth. This can be explained postulating an underlying c^{gr} FE domain ($\bar{\varepsilon}^{FM} = \bar{\varepsilon}^{FM}_{growth} = \bar{\varepsilon}_c = 0\%$) or underlying a_1^{gr}, a_1^{gr}/c^{gr} or a_1^{gr}/a_2^{gr} domains with small strain transfer ($\bar{\varepsilon}^{FM} = \delta\bar{\varepsilon}_{c,a_1,a_2}$) so that the ferroelastic induced magnetoelastic anisotropy does not overcome exchange and magnetostatic energies[2]. After cooling the sample down to 60 K and returning to 320 K we observe a γ FM domain pattern (Figure 3(a)) in reminiscence of an underlying a_1/a_2 FE domain pattern present at growth time and/or after the thermal excursion. As the strain transfer at growth time is significantly smaller than that due to temperature-induced FE phase changes[8] we conclude that after the thermal cycle the underlying FE domain state is indeed a_1^T/a_2^T. The a_1^T and a_2^T domains locally drive the magnetic easy axis and the magnetization[2] for the top Fe layer along $[010]_{pc}$ and $[100]_{pc}$, respectively (white and blue coded regions in Figure 3(a)).

The FE domain state at growth time can be obtained once the FE domain state after the thermal cycling is known (a_1^T/a_2^T). From the different possibilities, the following options can be discarded when considering the effects that the application of a voltage (after the thermal cycle) leading to a FE a_1^V/c^V domain state for BTO has on the FM magnetic domain pattern of Fe;

- An a_1^{gr}/a_2^{gr} FE domain state with FE domain walls along $[110]_{pc}$: This is not our case as we do not observe FM domain walls along $[110]_{pc}$ at any time after the thermal cycle or after the V application. Such domains were seen in other studies, for example by Lahtinen *et al.* (Ref. 8).
- An $a_2^{gr}/c^{gr\prime}$ FE domain state with FE domain walls along $[010]_{pc}$: As in the previous case, the absence of FM domain walls along $[010]_{pc}$ excludes this option.
- A pure a_1^{gr} or c^{gr} FE state: Only two FM domain types would be present after the V is applied.
- An a_1^{gr}/a_2^{gr} FE domain state with FE domain walls along $[\bar{1}10]_{pc}$: In that case the FE domain history for BTO would be the following; $a_1^{gr}/a_2^{gr} \rightarrow a_1^T/a_1^T \rightarrow a_1^V/c^V$. Figure S3 shows a

differential strain analysis so to determine $\bar{\varepsilon}^{FM}$ and consequently the easy magnetic axis and magnetization direction expected at each step, i.e. after thermal cycle and application of V. For the sake of clarity we consider $\delta = 0.1$ (higher limit of reported values[1, 2, 7, 8] and note that any non-zero value smaller than 0.1 would also lead to the same results. Our analysis shows that on top of a_1^V domains the magnetization direction would be aligned along $[010]_{pc}$ ($\bar{\varepsilon}^{FM} > 0$) independently of whether at growth time the FE domain underneath was a_1^{gr} or a_2^{gr}. On top of c^V the magnetization direction would alternate along $[010]_{pc}$ and $[100]_{pc}$ due to the fact that $\bar{\varepsilon}^{FM}$ is positive (negative) for Fe regions on top of a_2^{gr} (a_1^{gr}) domains at growth time. Hence the expected FM domain pattern on top of BTO a_1^V and c^V domains would be α and γ-FM like, respectively. β-like FM regions would not appear as in that case it would be necessary that $\bar{\varepsilon}^{FM} < 0$ for the whole Fe region on top of the new a_1^V and/or c^V domains. This is in contradiction with our experimental observations, see for example Figure 3 (c,d).

We hence conclude that at growth time the initial FE domain state was a_1^{gr}/c^{gr} with domain walls along $[100]_{pc}$

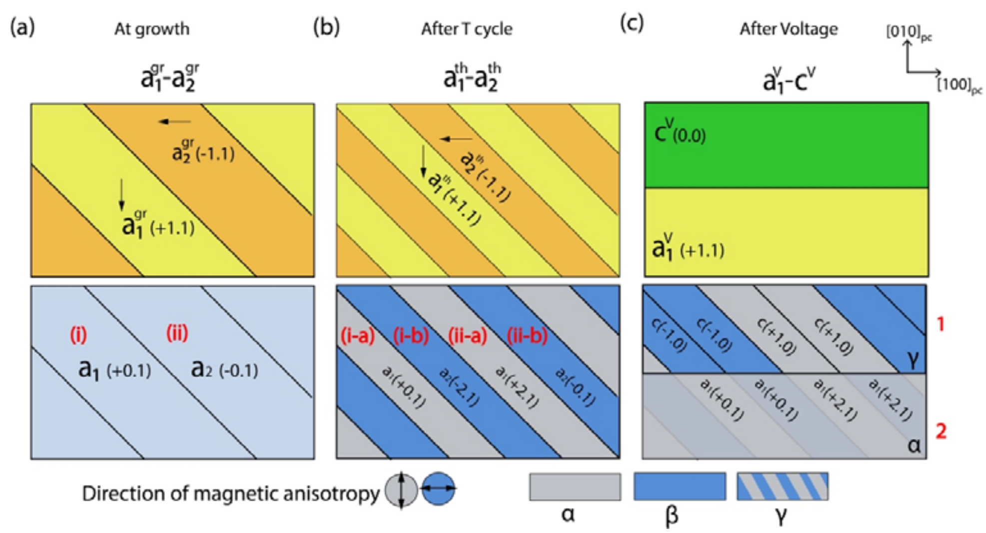

Figure S3 Differential strain analysis proving that an $\boldsymbol{a_1^{gr}}$/ $\boldsymbol{a_2^{gr}}$ FE domain pattern for BTO at growth time cannot explain the observation of $\boldsymbol{\alpha}$, $\boldsymbol{\beta}$ and $\boldsymbol{\gamma}$-FM like domain for Fe after a thermal cycle and application of a Voltage leading to $\boldsymbol{a_1^V/c^V}$. a), panels show the FE state for BTO (top) and expected FM state for Fe (bottom) after growth a), after the thermal treatment b) and after the application of a voltage c), respectively. Values in between brackets correspond to the differential strain for the BTO ($\bar{\boldsymbol{\varepsilon}}$) and for the Fe films ($\bar{\boldsymbol{\varepsilon}}^{\boldsymbol{FM}}$), respectively. Based on the local values $\bar{\boldsymbol{\varepsilon}}^{\boldsymbol{FM}}$ the magnetic easy axis and hence the orientation of the magnetization for the different domains can be deduced. Our results show that an $\boldsymbol{a_1^{gr}}$/ $\boldsymbol{a_2^{gr}}$domain state for BTO lead to $\boldsymbol{\alpha}$ and $\boldsymbol{\gamma}$ FM domains but not to $\boldsymbol{\beta}$ ones, contrary to experimental evidence.

Once the FE domain state of BTO at growth time and after the thermal cycle are known we can perform a differential strain analysis to determine the local changes of the magnetic easy axis and magnetization direction orientation as V is applied. These “predictions” can be then compared to experimental observations to validate our deductions. Figure S4 shows such analysis for the case a voltage is applied right after the thermal cycle leading to an a_1^V/c^V FE state for BTO. In that case the FE domain history would be $a_1^{gr}/c^{gr} \rightarrow a_1^T/a_2^T \rightarrow a_1^V/c^V$. The $c^{gr} \rightarrow a_1^T/a_2^T \rightarrow a_1^V/c^V$ case is depicted in panels (a, c, e) while the $a_1^{gr} \rightarrow a_1^T/a_2^T \rightarrow a_1^V/c^V$ is analysed in panels (b,d,f).

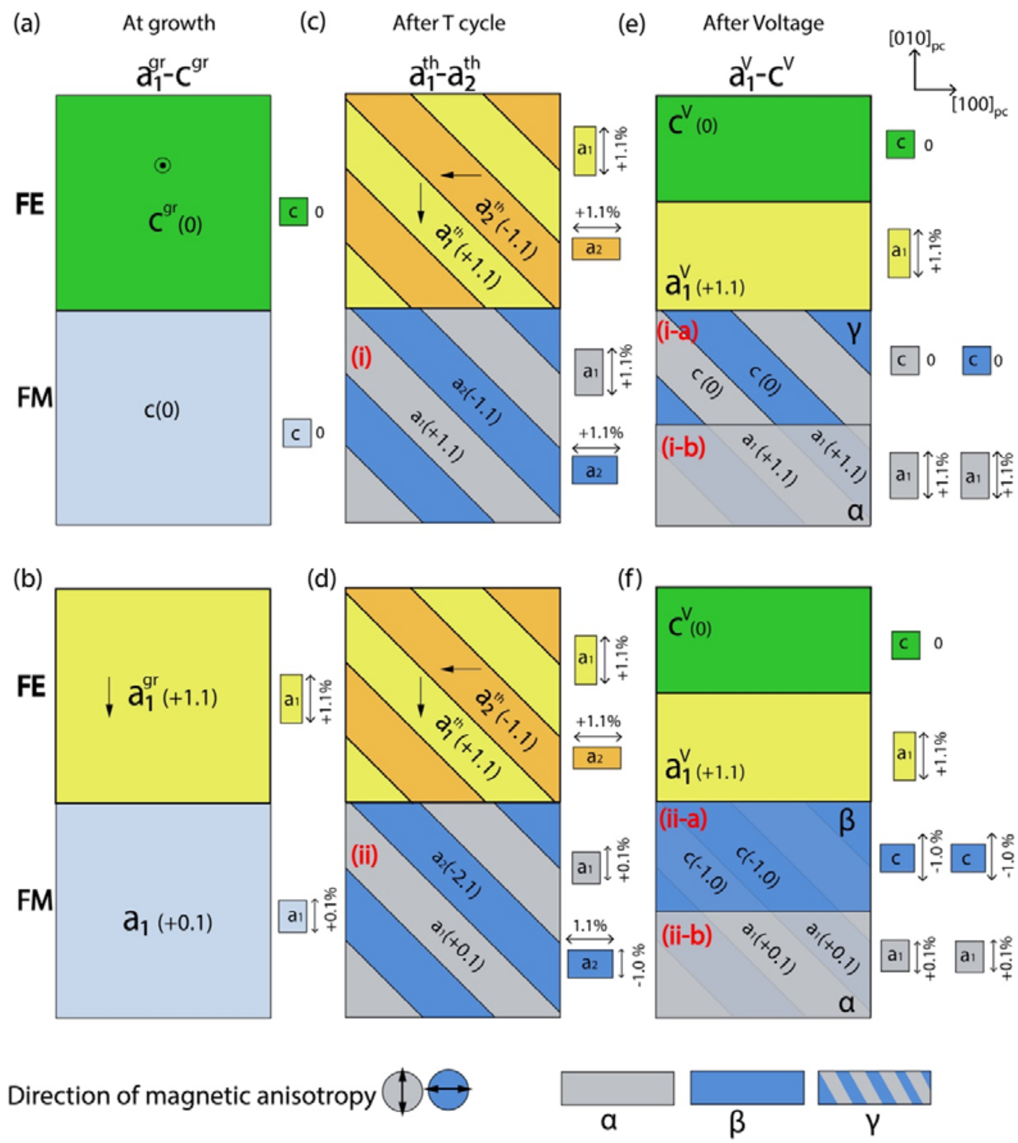

Figure S4 Differential strain analysis for the case of an $\boldsymbol{a_1^{gr}/c^{gr}}$ FE domain sate for BTO at growth time. panels show the FE state for BTO (top) and expected FM state for Fe (bottom) after growth (a,b), after the thermal treatment (c, d) and after the application of a voltage (e, f), respectively. Values in between brackets correspond to the differential strain for the BTO ($\bar{\varepsilon}$) and for the Fe films ($\bar{\boldsymbol{\varepsilon}}^{\boldsymbol{FM}}$), respectively. Based on the local values $\bar{\boldsymbol{\varepsilon}}^{\boldsymbol{FM}}$ the magnetic easy axis and hence the orientation of the magnetization for the different domains can be deduced. Strain orientation and strength is depicted at the right side of each panel for BTO and Fe for given FE BTO domains c, $\boldsymbol{a_1}$, or $\boldsymbol{a_2}$.

The differential strain analysis predicts that the application of a voltage leading to an a_1^V/c^V FE domain state must lead for Fe to FM domains alike to those we have experimentally observed, i.e. α, β, and γ FM domains. While the direction of the magnetization or the magnetic easy axis is clearly stabilized by the sign of $\bar{\varepsilon}^{FM}$ at each domain, the case of the γ pattern for c^V deserves some clarification as in such case $\bar{\varepsilon}^{FM}$ = 0. For that region $\bar{\varepsilon}^{FM}$ alternated sign before applying the voltage, thus defining magnetic easy axis along two orthogonal directions, i.e. $[100]_{pc}$ and $[010]_{pc}$. The application of V leads to an underlying FE c^V. As the state at growth time was also c^{gr}, the differential strain for Fe on top of this domain is $\bar{\varepsilon}^{FM}$ = 0 but the magnetization keeps its earlier orientation likely due to magnetic domain wall pinning / friction.

The origin of β- and γ-like FM regions is univocally determined in terms of strain history. While they both sit on top of FE c^V domains they had different FE domains at growth time i.e.;

For β; $a_1^{gr} \rightarrow a_1^T/a_2^T \rightarrow c^V$

For γ; $c^{gr} \rightarrow a_1^T/a_2^T \rightarrow c^V$

On the contrary α FM domains can be obtained following two different paths with opposite FE domains state at growth time and after the application of a voltage i.e.;

$$\text{either } a_1^{gr} \rightarrow a_1^T/a_2^T \rightarrow a_1^V \text{ or}$$

$$c^{gr} \rightarrow a_1^T/a_2^T \rightarrow a_1^V$$

We note that the comparison between Figure 3(d) and 4(a), both obtained at V = +170 V but at different azimuthal angles show that new α are made of smaller domains with magnetization direction alternating along the two possible $[010]_{pc}$ and $[0\bar{1}0]_{pc}$ directions of the magnetic easy axis. On the contrary new β FM domains are single domain with magnetization direction along $[100]_{pc}$, i.e. no domains with magnetization along $[\bar{1}00]_{pc}$. This can be explained by considering that most of the magnetization within the field of view is oriented along $[100]_{pc}$ so that the orientation of the magnetization of new β domains along this very same direction is energetically favourable. For new α domains with magnetization oriented orthogonally to $[100]_{pc}$ there is no difference in terms of energy for domains aligned along $[010]_{pc}$ or $[0\bar{1}0]_{pc}$, hence both domains nucleate.

Further increasing the V leads to the growth of c^V FE domains in BTO at expenses of a_1^V ones. Eventually, for large enough voltages, a_1^V completely disappear leading to a single c^V state for BTO, i.e. $a_1^V/c^V \rightarrow c^V$. This case is considered in Figure S5 where panels a) and b) correspond to the initial state and panels c) and d) to the final one. The differential strain analysis shows that a change of the magnetization orientation after $a_1^V \rightarrow c^V$ is expected only for these regions which at growth time sit on top of a_1^{gr} FE domain. In that case, M rotates from $[010]_{pc}$ /$[0\bar{1}0]_{pc}$ to $[100]_{pc}$ i.e. α to β FM domain transition.

The differential strain analysis in terms of magnetoelastic anisotropy changes allow us to explainour experimental observations, namely:

- γ FM state after thermal treatment; originating from $a_1^{gr}/c^{gr} \rightarrow a_1^T/a_2^T$ FE transitions
- Persistance of γ FM state after applying a voltage
- Coexistance of α, β, and γ FM domains after applying a voltage

- γ to α transitions; $a_1^T/a_2^T \rightarrow a_1^V$
- γ to β transitions; $a_1^T/a_2^T \rightarrow c^V$ for a_1^{gr} at growth time
- α to β transitions; $a_1^V \rightarrow c^V$ for a_1^{gr} at growth time

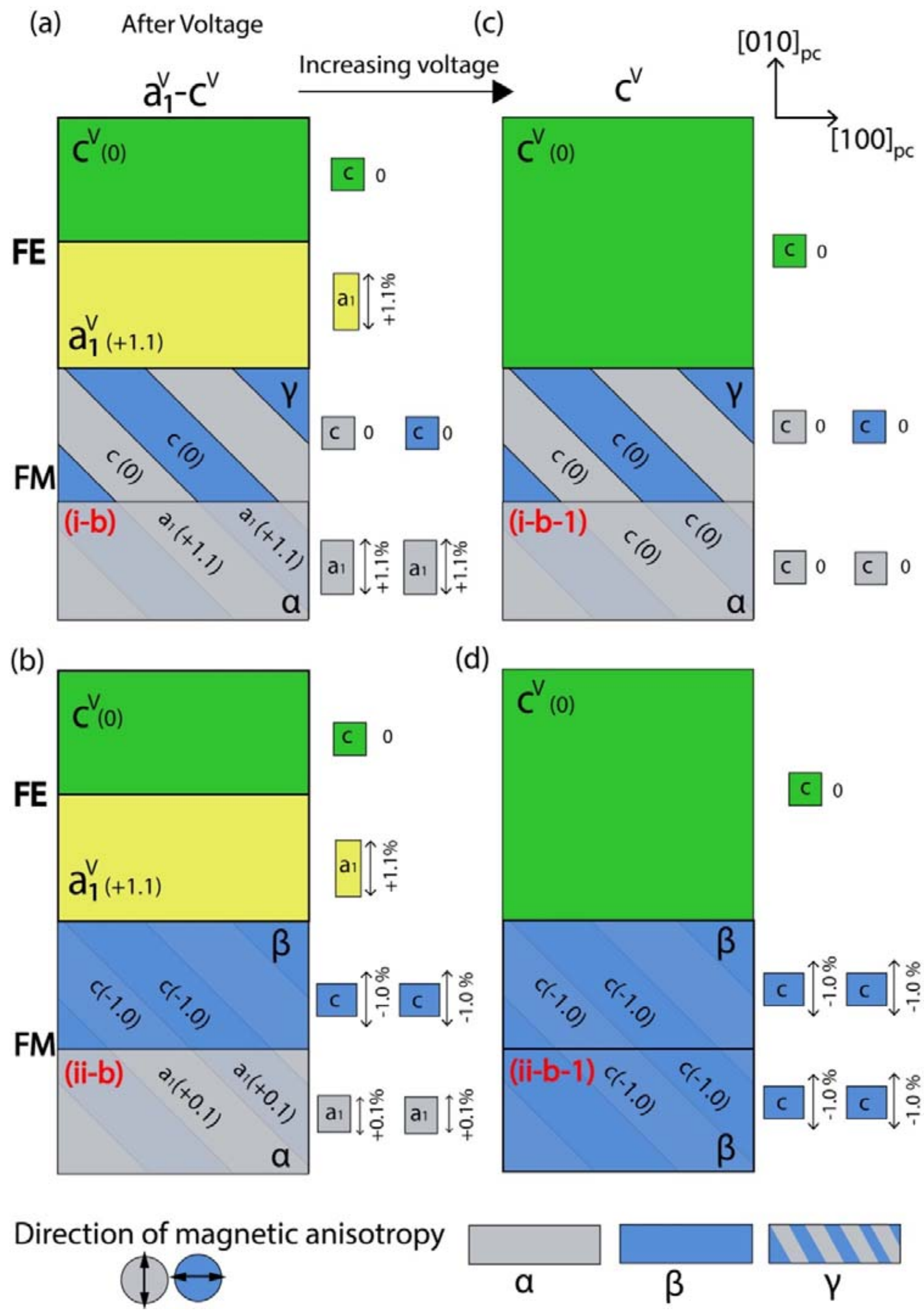

Figure S5 Differential strain analysis so to predict the FM domain state for a voltage large enough so to lead to a single c FE domain state for the underlying BTO substrate. (a,b) intermediate $\boldsymbol{a_1^V/c^V}$ FE state as the one depicted in Figure S4(c, f). (c, d) for complete $\boldsymbol{c^V}$ FE state.

4.- Electric field induced extension of long range ferromagnetic ordering to lower Fe thicknesses

As explained within the main text we observe an extension of long range ferromagnetic ordering towards lower thickness Fe regions of the wedge after applying a voltage to the BTO substrate. This happens for β regions only. This can be seen in Figure 3(c,d) and Figure 4 where we can identify two different FM states prior to the β one, namely,

i) β originating from a γ domain (Figure 3(c,d))
ii) β originating from an α domain (Figure 4(b,c))

Based on the differential strain analysis reported in section 3 we can identify the FE domain history of the BTO substrate underneath these areas, being respectively;

i) $a_1^{gr} \rightarrow a_1^T/a_2^T \rightarrow c^{\vee}$ and,
ii) $a_1^{gr} \rightarrow a_1^T/a_2^T \rightarrow a_1^V \rightarrow c^{\vee}$
In both cases Fe on top is compressed along $[010]_{pc}$ by ca. 1.1% as compare to its initial strain state.

According to our analysis α FM domains might also show a sizable tensile strain of the order of ca. 1.1% (see Figure S4(e)). The modification of the magnetic anisotropy energy in that case would be similar to that due to the compression experience at β so that an extension of long-range FM order due to an increase of T_p should also be expected. We note at that point that α regions can originate following different FE histories for the BTO underneath;

a) $c^{gr} \rightarrow a_1^T/a_2^T \rightarrow a_1^V$ leading to a tensile stress on Fe along $[010]_{pc}$ of ca. 1.1%, or
b) $a_1^{gr} \rightarrow a_1^T/a_2^T \rightarrow a_1^V$ leading to a tensile stress on Fe along $[010]_{pc}$ much smaller, i.e. ca. 0.1%
c) $c^{gr} \rightarrow a_1^T/a_2^T \rightarrow a_1^V \rightarrow c^{\vee}$ with no strain.

Experimentally we observed that α domains tend to disappear (converting into β) as Voltages is cycled from 170 V to -170 V (Figure 4). This is only expected for FM regions with underlying $a_1^{gr} \rightarrow a_1^T/a_2^T \rightarrow a_1^V$ FE history followed by a conversion to $c^{\vee}$ (case b) for which the with strain much lower than that experience for Fe depicting FM β-like regions.

Hence we conclude that there is a direct correlation between the extension of long range FM ordering towards lower Fe thicknesses and the strain state of Fe, which of course, depends on the strain history of the underlying BTO substrate.

5.-Electric field induced change in the critical thickness for long-range FM

Figure S6 shows XMCD images obtained at +170 V (panel a) -170 V (panel b) showing 5 different regions for which we have observed an electric-field induced extension of the FM region towards lower Fe thicknesses.

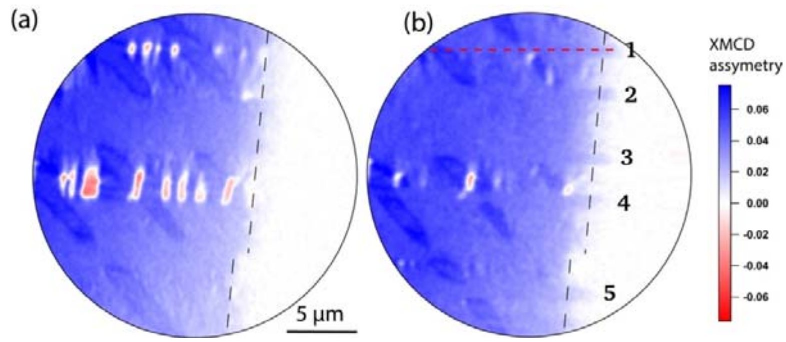

Figure S6 XMCD images (field of view of 25 μm) obtained at the Fe L_3 edge (707.8 eV) at 320 K and (a) V= +170V and (b) V= -170 V. Number 1 to 5 indicate β FM like regions which show an extension of the onset of long-range FM towards lower t_{Fe} regions. XMCD profiles as function of the applied Voltage across these lines is depicted in Figure S7.

Figure S7 shows a 2D plot for each of these 5 regions where we plot the XMCD line profile as function of Voltage following a line parallel to that depicted for region 1 (red dashed line) in Figure S6. Vertical axis corresponds to a sequential application of Voltage from 170 V to -170 V (bottom to top). The Horizontal axis corresponds to the pixel position across the red line (512 pixels correspond to 25 μm). Black/white contrast corresponding to an XMCD ranging 0 and 0.05 has been selected so to enhance the formation of extended FM regions.

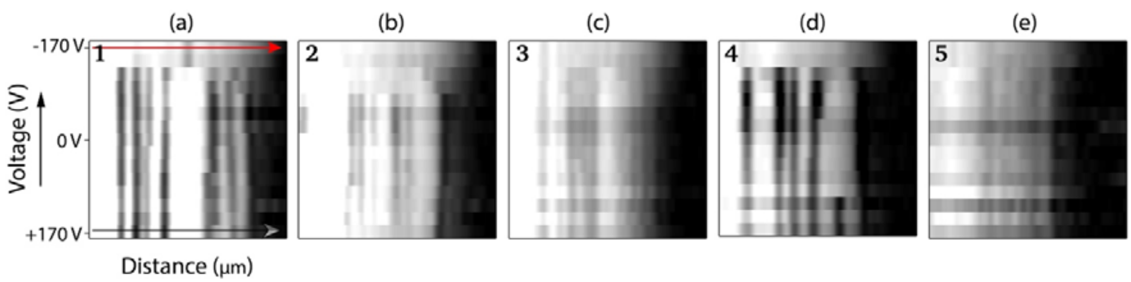

Figure S7 2D XMCD Vs Voltage plots for red dashed lines labelled 1 to 5 in figure S6. Horizontal axis corresponds to the pixel position across the line. Vertical axis is the V which runs from 170 V (down) to -170 V (up). The long-range FM region (bright contrast) extends into the non FM one as V approached -170 V.

In order to precisely determine how much t_{FM} has changed we compare in Figure S8 XMCD line profiles obtained before (V = +170 V, black lines) and after (V = -170 V, red lines) the extension of long-range FM region towards lower t_{Fe} takes place. Based on this analysis we determine an average expansion of the FM region on these specific positions of ca. 1.3 μm. Such extension towards lower t_{Fe}, corresponds to a decrease of t_{FM} of ca. 1Å as deduced when considering the dependence of the XAS intensity on the Fe thickness (ca. 0.7 Å/μm) depicted in Figure 1(e).

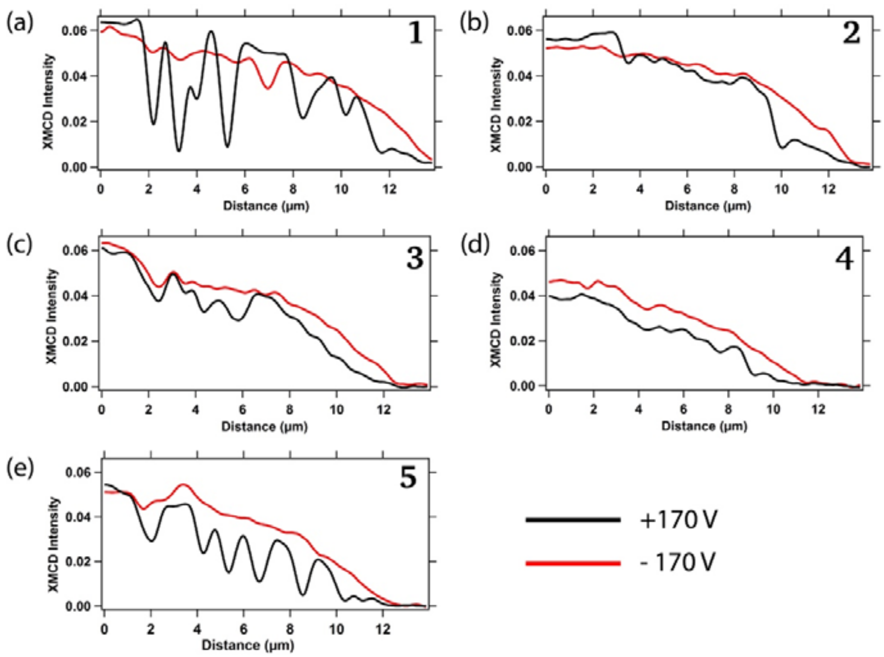

Figure S8 XMCD line profiles at 170 V (black line) and -170 V (red line) across red-dashed lines depicted in Figure S6. The onset of long-range FM (non-zero XMCD) extends towards lower $t_{Fe.}$

6.- Change in T_C necessary to decrease t_{FM} by ca. 1 Å

In order to know the change in the Curie temperature necessary to induce a decrease of t_{FM} by ca. 1 Å we have performed temperature dependent XMCD measurements on an Fe wedge film on BTO similar to that for which we report on electric field induced modification of t_{FM}, see Figure S9. This film shows also a similar t_{FM} at 320 K. As shown in Figure S9 increasing the temperature from 80 K to 340 K (260 K variation) leads to an extension of the FM region within the 25 µm field of view of ca. 1 µm which an associated decrease of t_{FM} of ca. 5 Å. Hence, if an electric-field induced change of T_c is invoked to explain our experimental observation of a decrease in t_{FM} of ca. 1 Å, such change should correspond to an increase of T_c of about 50 K.

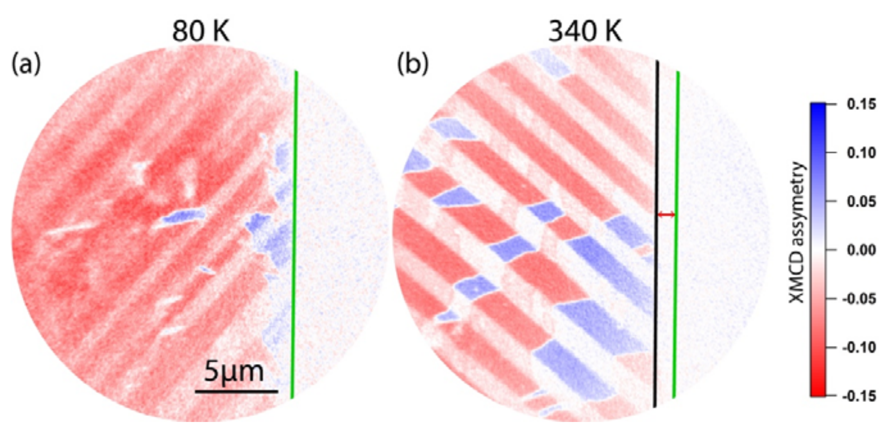

Figure S9 XMCD images (25 µm field of view) obtained on a 0-3 nm Fe wedge deposited on top of BTO. a) and b) images have been obtained at 80 K and 340 K, respectively. Green and black lines mark the position corresponding to the onset of FM, i.e. t_{FM} (80K) and t_{FM} (340K) respectively.

As explained within the text an electric field induced change of T_c of about 50 K is not compatible with experimental and theoretical evidences. Hence, the extension of long-range FM is interpreted as an electric field induced change of about 50 K of the transition temperature T_p separating superparamagnetic and superferromagnetic regimes.

References

1. T.H.E. Lahtinen, K.J.A. Franke and S. v. Dijken, Sci. Rep. **2**, 258 (2012).
2. T. N. Yang, J.-M. Hu, C. W. Nan and L. Q. Chen, Appl. Phys. Lett. **104** 202402 (2014).
3. E. du Trémolet de Lacherisseie, D. Gignoux and M. Schlenker, *Magnetism fundamentals*. (Springer, Boston, 2005).
4. D. Sander, Rep. Prog. Phys. **62**, (1999).
5. E. d. T. d. Lacheisserie, J. Magn. Magn. Mater. **13**, 307 (1979).
6. L. C. Phillips, R.O. Cherifi, V. Ivanovskaya, A. Zobelli, I.C. Infante, E. Jacquet, N. Guiblin, A.A. Ünal, F. Kronast, B. Dkhil, A. Barthélémy, M. Bibes and S. Valencia, Sci. Rep. **5**, (2015).
7. R. Streubel, D. Köhler, R. Schäfer and L. M. Eng, Phys. Rev. B **87**, 054410 (2013).
8. T.H.E. Lathinen and S. v. Dijken, Appl. Phys. Lett. **102**, 112406 (2013).
9. O. Boulle, J. Vogel, H. Yang, S. Pizzini, D. de Souza Chaves, A. Locatelli, T. O. Menteş, A. Sala, L. D. Buda-Prejbeanu and O. Klein, Nat. Nanotechnol. **11** (5), (2016).
10. R. Chopdekar, V. K. Malik, A. Fraile Rodríguez, L. Le Guyader, Y. Takamura, A. Scholl, D. Stender, C. W. Schneider, C. Bernhard, F. Nolting and L. J. Heyderman, Phys. Rev. B **86**, 014408 (2012).